CFD Study of Thermal Detection in a Closed Compartment Subject to External Fires

S. KUMAR and R. CHITTY
Fire Research Station, Building Research Establishment, Garston, Watford, U.K.

ABSTRACT

The CFD models JASMINE and SOFIE have been used to simulate the convection currents and thermal conditions inside one steel compartment due to a fire in an adjacent compartment. The impact, on the thermal environment inside the steel compartment, of the positioning of the adjacent fire in both 'side-heated' and 'bottom-heated' configurations has been examined.

For the side-heated configuration, the predicted thermal conditions inside the steel compartment, based on a standard 'hydrocarbon' specification for the fire source in the adjacent compartment, have been compared with a full-scale experiment using a liquid fuel spray burner as the fire source. For the bottom-heated configuration, since there were no experimental data available, the predicted flow patterns inside the steel compartment were supported by additional two-dimensional steady-state CFD simulations in a 3m high rectangular geometry for aspect ratios ranging from 1:1 to 1:8 by enforcing both horizontal and vertical temperature gradients.

KEY WORDS: CFD, JASMINE, SOFIE, offshore structure, steel compartment, side-heated configuration, bottom-heated configuration

INTRODUCTION

For many years natural convection in enclosures has been of considerable practical interest to many widely diverse engineering applications, such as space cooling and heating in environmental flows, fires in buildings, tunnels and off-shore structures, nuclear reactor systems, material processing, solar energy, electronic equipment, etc. Research in confined natural convection in rectangular configurations has covered two- and three- dimensional tall ($A>>1$) and slender ($A<<1$) rectangular cavities and enclosures, A being the height-to-width aspect ratio of the enclosed space.

Much of the attention has been centred on two basic modes of natural convection, one involving differential heating from the side and the other involving heating from below. In the case of differentially heated cavities involving hot and cold vertical sides, the horizontal sides are normally considered to be adiabatic. In the second case where the cavity or enclosure is heated from below, the vertical sides have been considered to be adiabatic. Ostrach [1] has provided a fairly comprehensive review of the current state of research on differentially heated cavities. More recently Hanjalic & co-workers [2,3] have investigated the suitability of single point turbulent models for side-heated enclosures involving horizontal temperature gradient and bottom-heated enclosures involving vertical temperature gradient. However, little attention has been paid to the mixed-mode natural convection, involving both horizontal and vertical temperature gradients, which is the topic of interest in the present study.

This paper examines the impact, on thermal conditions inside a steel compartment of an offshore structure, of a fire in an adjacent compartment. The fire compartment will hereafter be referred to as Compartment 1 and the adjacent compartment as Compartment 2. The parameters considered in this study are:

- characterisation of the thermal response of a fire in the fire compartment based on the standard hydrocarbon time-temperature curve or from a full-scale fire experiment, and
- the effect of positioning of the adjacent fire compartment in side-heated or bottom-heated configuration.

The purpose of the study was to predict 'detection times' for 'heat detectors' at some pre-specified locations inside Compartment 2 due to a fire in the adjacent Compartment 1. In the present study, the 'detection time' has been defined as the time when the local gas temperature at a pre-specified 'heat detector' location has reached 68°C. The radiative exchange between the hot and cold surfaces within Compartment 2, which may have some influence on 'detection times', has been ignored here for simplicity. However, a heat transfer coefficient approach has been used to account for the effect of radiative and convective heat losses from the buoyant heated air to the solid boundaries of this compartment.

THE SCENARIOS

Figure 1 shows the plan of Compartment 2 of the two-compartmented offshore steel structure under consideration along with its overall dimensions and the locations of 1mm-sheathed thermocouples positioned 100mm below the ceiling. For brevity, other instrumentation is not shown here. The structure consists of a fire compartment (Compartment 1) and the adjacent Compartment 2 with stiffeners on the internal side walls and a mesh structure (made of beams and girders) close to the deckhead, and a storage rack which occupies approximately a quarter of the compartment floor area. The external surfaces of Compartment 2 were specified as constant temperatures, which were 25°C for the deck, deckhead and bulkhead D, 20°C for bulkhead A and 7°C for bulkhead B (adjacent to the sea). The temperature of the ambient air was taken to be 20°C.

Three different fire scenarios, hereafter referred to as Scenarios A, B and C, were considered under two geometrical configurations. Scenarios A and B correspond to the side-heated

configuration where the fire compartment is situated horizontally adjacent to Compartment 2. Scenario C corresponds to the bottom-heated configuration where the fire compartment is situated vertically below Compartment 2. The schematic representation of the two geometrical configurations is shown in figure 2. The detailed description of each scenario is given below:

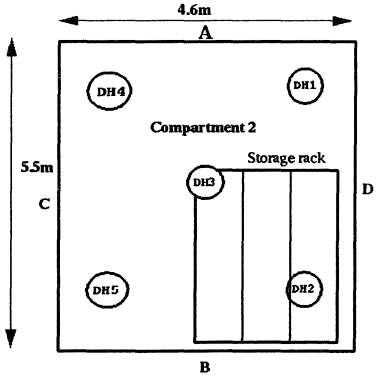

FIGURE 1 Plan of Compartment 2 with 'detector' locations DH1 – DH5, 100 mm below the deckhead

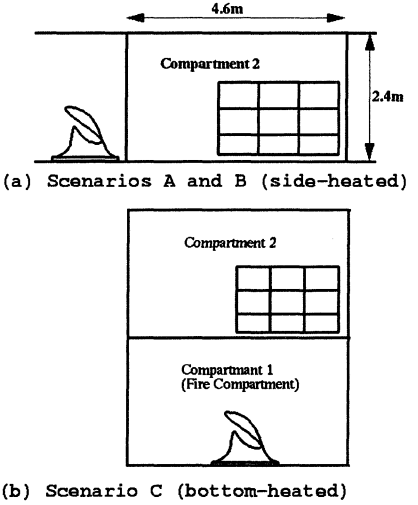

FIGURE 2 Geometrical configuration of offshore steel structure

Scenario A

Scenario A corresponds to the side-heated configuration of Compartment 2 with respect to Compartment 1 (fire compartment). The transient thermal response of the common bulkhead, joining the fire compartment to the adjacent compartment, is characterised by the standard hydrocarbon time-temperature exposure curve. The hydrocarbon curve is representative of a flashed-over fire scenario characterised by a uniform heat source with a temperature rise of 1000°C above ambient and duration of 1 hour. The hydrocarbon fire test was developed so that the elements of a structure could be exposed to an initial fast-growing intense fire representing a fuel spill (such as that from a crashed helicopter), followed by a slightly less intense but longer duration phase representing engulfment in a burning fuel slick. It has also been assumed that the fire is fully developed in the compartment adjacent to the steel compartment and that there are no significant temperature gradients over the surface of the common bulkhead C. The data based on this curve were used by THELMA [4] for predicting the heat transfer through a section of the bulkhead (including a stiffener) and to estimate the temperature of the bulkhead on the exposed side of Compartment 2. THELMA is a two-dimensional finite-element computer model developed at the BRE Fire Research Station. The temperature predicted by THELMA of the bulkhead C was then used by the CFD models [5,6] as a boundary condition to predict the detailed (convective) air flow patterns and the consequential temperature rise at various locations inside Compartment 2. The storage rack and internal stiffeners on the bulkheads and deckhead are modelled by blocking the faces of the numerical grid cells.

Scenario B

Scenario B is identical to Scenario A in the geometrical configuration of Compartment 1 and Compartment 2, but differs in the specification of the time-temperature response of the common bulkhead. In contrast to Scenario A where this is determined from the standard hydrocarbon time-temperature fire exposure curve, in Scenario B the measured temperature from a full-scale experiment has been used to specify the time-temperature curve for the common bulkhead. This scenario provides a test case for the verification of the CFD model against the data from a full-scale fire experiment. It should be noted that the fire source used for scenario A, characterised by the standard hydrocarbon curve, is more severe than the liquid fuel spray fire (with a nominal heat-release rate of 1 MW) used in the full-scale experiment for scenario B.

Scenario C

Scenario C corresponds to the bottom-heated configuration of Compartment 2 where the heating is from the fire compartment below (see figure 2). The transient thermal response of the Compartment 2 deck, adjoining the fire compartment below it, is characterised, as in Scenario A, by the standard hydrocarbon time-temperature exposure curve.

Similar to Scenario A, it used the standard hydrocarbon time-temperature curve and the computer model THELMA to calculate the time-temperature history of the deckhead of Compartment 1 (connecting to the deck of Compartment 2). The time-temperature history predicted by THELMA was then used by the CFD model to predict the air movement and thermal conditions inside the steel compartment.

EXPERIMENTAL DETAILS FOR SCENARIO B

A series of full-scale experiments were carried out in an offshore test facility, and the effect of the fire on the steel structure was investigated. The experiment attaining the fully developed state was found most appropriate for the verification of the CFD model due to the following reasons. In this experiment the fire was produced by a liquid fuel spray burner in the fire compartment and was positioned centrally, opposite the common bulkhead C joining Compartment 1 (fire compartment) to Compartment 2. This burner arrangement gave rise to a 'hot spot' over an area of approximately 2m square on the centre of the common bulkhead. Four thermocouples were mounted within the 2m central area on the unexposed surface (Compartment 2 side) of the bulkhead to characterise the transient thermal response of the fire source on this surface.

1mm-sheathed thermocouples were used for measuring the air temperatures inside the test facility. Although less accurate than fine-wire thermocouples (typically, 200 μm diameter), they were used for robustness rather than accuracy because the experiments required the use of a water spray with high delivery rate for cooling the test facility from a flashed-over fire. Once installed, the same instrumentation was to be used for comparing the data from several experiments in the same test series. Clearly fine-wire thermocouples are more susceptible to breakage than sheathed thermocouples in such a harsh environment.

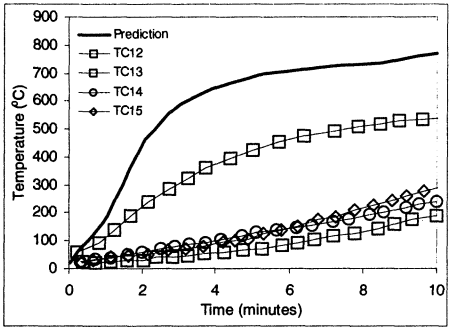

FIGURE 3 Comparison of the predicted and measured time-temperature histories on bulkhead C (Thermocouples 12-15 are on unexposed side of bulkhead C)

The time-temperature history of four thermocouples attached to the common bulkhead is compared in figure 3 with the THELMA predictions using the standard hydrocarbon time-temperature curve. It is clear from this figure that the time-temperature history of thermocouple 12 was qualitatively similar to the hydrocarbon curve. The lower thermal response of the other three thermocouples indicates that they might have come off the surface of the bulkhead and therefore could not realistically represent the thermal response of the fire source.

DETAILS OF THE NUMERICAL SIMULATIONS

The transient response of the fire source was modelled by using the time-temperature history of thermocouple 12 on the 2m square area located centrally on the unexposed surface (Compartment 2 side) of the common bulkhead.

For all three scenarios, a total of 35,000 numerical grid cells and a time step of one second were used for each CFD simulation. The numerical grid was designed such as to ensure high grid resolution in regions with steep temperature gradients, for example close to the common bulkhead and the deckhead. For Scenario A, a grid sensitivity study was undertaken where the number of grid cells was increased from 35,000 cells to 110,000 cells. Both standard (high Reynolds number) k-ε turbulence model with buoyancy modification and its low Reynolds number version based on the work by Launder and Sharma [7] were used in the simulations.

For scenarios A and C the numerical simulations were continued for the duration of 10 minutes and scenario B for 12 minutes, at which point the air temperatures had reached 68°C at all the deckhead temperature locations. The detailed temperature flow-field information was stored at 10 seconds intervals.

For Scenario C, corresponding to the bottom-heated configuration, since there was no experimental information available, two-dimensional steady-state CFD simulations were performed for a 3m high and 12 m wide rectangular geometry (giving an aspect ratio 1:4), using the first-order upwind formulation and the standard k-ε turbulence model. The rectangular geometry of 3 m x 12m was represented numerically by a 60 x 250 grid, giving a typical grid cell size of 0.05m and a cell aspect ratio of about 1:1. The bottom-side was set arbitrarily to a temperature of 100°C and the top-side to an ambient temperature of 20°C. The temperature of the vertical sides was varied between 20°C and 100°C.

To examine the influence of the wall functions on the buoyancy-induced convection-flow patterns, additional CFD simulations were carried out using the second-order hybrid difference formulation both for standard (high Reynolds number) k-ε turbulence model and low-Re k-ε turbulence model based on the work by Launder and Sharma [7]. The temperatures of the top and bottom sides were kept, as before, on 20°C and 100°C and vertical sides on 25°C. The influence of the aspect ratio of the rectangular geometry on the fluid flow was also examined by varying its width such as to give aspect ratios ranging between 1:1 and 1:8.

RESULTS AND DISCUSSION

For each scenario, time-temperature histories were plotted at the various temperature measurement locations used in the fire test. As an illustration, figure 4 provides a comparison of the time-temperature histories for the three scenarios at the simulated detector locations DH1 to DH5. It is worth noting here that the predicted time-temperature histories follow the hydrocarbon curve for scenarios A and C and experimental fire growth curve for scenario B. This is clearly evident from figure 3, where the predicted temperature on the unexposed side of bulkhead C uses the hydrocarbon curve and measured temperature from thermocouple 12 represents the fire growth behaviour.

A summary of the CFD predictions in the form of 'detection times' is provided in Table 1 for the three scenarios at the pre-specified temperature locations near the deckhead of Compartment 2. It should be noted that the 'detection time' corresponds to the time when the local air temperature has reached 68°C. For Scenario A the 'detection times' obtained from the fine grid study have also been included in the table. For Scenario B the measured detection times obtained from the full-scale experiment have also been included for model verification purposes. The measured detection time corresponds to the time of operation of the centrally-located heat

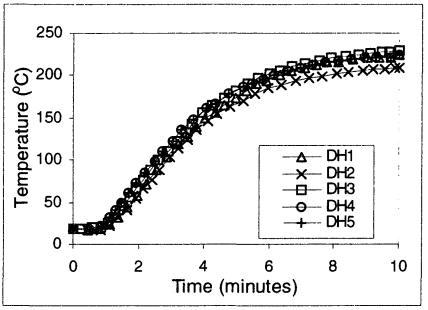

(a) Scenario A

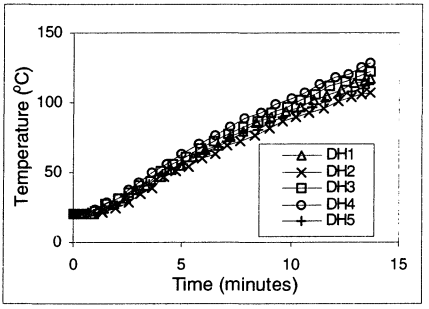

(b) Scenario B

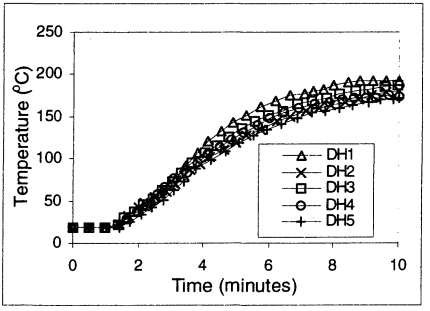

(c) Scenario C

FIGURE 4 Time-temperature histories for each scenario at simulated detector locations

detector or when a thermocouple had reached a temperature of 68°C (uncorrected) or 41°C after correction for conduction losses.

The discussion of results for individual fire scenarios follow next.

Scenario A

The effect of the grid refinement on the 'detection times' is summarised in Table 1. It can be seen that the 'detection times' are reasonably insensitive to the refinement of the numerical grid from 35,000 cells to 110,000 cells. The differences in the 'detection times' at the deckhead locations DH1 to DH5 can be seen to be less than 4% at the cold wall and less than 1% near the heated wall, demonstrating the robustness of the numerical solution and giving confidence in the coarser grid predictions.

TABLE 1. 'Detection times' (s) at locations DH1 to DH5

Scenario		Detector locations				
		DH1	DH2	DH3	DH4	DH5
Simulation	A-prediction (coarse grid)	128	131	117	110	110
	A-prediction (fine grid)	133	134	122	111	111
	B-prediction	386	420	360	378	391
Experiment	Heat detector at DH3			421		
	TC-uncorrected (time to 68°C)	802	728	703	506	502
	TC-corrected (time to 41°C)	355	325	288	198	310
Simulation	C-prediction	167	167	170	170	185

Figure 5 shows the isotherms predicted by the CFD model on a plane through the centre of the unobstructed side of Compartment 2. The predictions are compared with those reported by Markatos and Pericleous [8]. It can be seen that the features at bulkhead C (hot wall) and bulkhead D (cold wall) are similar. The differences in the flow patterns in the upper part of Compartment 2 could be attributed to the significant heat losses to the deckhead in the present study as compared to the adiabatic ceiling used by Markatos and Pericleous [8].

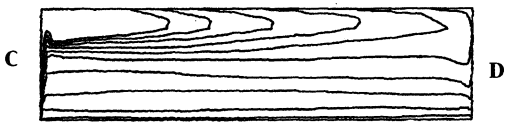

(a) Isotherms 1.2 m from bulkhead A inside compartment 2

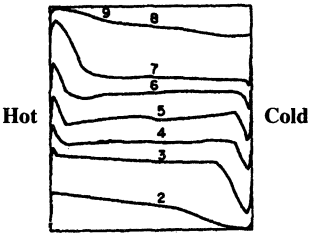

(b) Isotherms in a 2D side-heated cavity

FIGURE 5 Comparison of predicted isotherms on a vertical plane, 1.2 m from bulkhead A, with 2D side-heated cavity predictions from Ref. 8

Scenario B

It should be noted that the burner arrangement used in the fire compartment provided a 'hot spot' on the bulkhead. This observation is in contrast to the uniform bulkhead temperature assumption implicit in the standard hydrocarbon test time-temperature curve used for Scenarios A and C. Comparison of the measured bulkhead temperatures to THELMA predictions based on the hydrocarbon curve (see figure 3) shows that the fire achieved in the fire test is not as severe as represented by the hydrocarbon curve.

Table 1 provides the comparison of the predicted 'detection times' for Scenario B with measurements at the deckhead locations DH1 to DH5. The differences between predictions and measurements can be attributed to the use of 1mm sheathed-thermocouples in the test. It would have been desirable to use fine wire thermocouples; however this would have been incompatible with the robustness required for the water spray tests. Because of their size, the thermocouples suffer from large conduction losses along the length to their support (a large thermal mass). Consequently, the temperature measured by such a thermocouple is significantly lower than the temperature of the surrounding air. The data from the fire test has been processed to account for the error caused by conduction heat losses. By correcting for the conduction losses, the measured 'detection times' based on the lower recorded thermocouple temperatures are in reasonably good agreement with the CFD predictions. An expression to allow for the correction to thermocouple temperatures for these losses is described in the appendix.

Scenario C

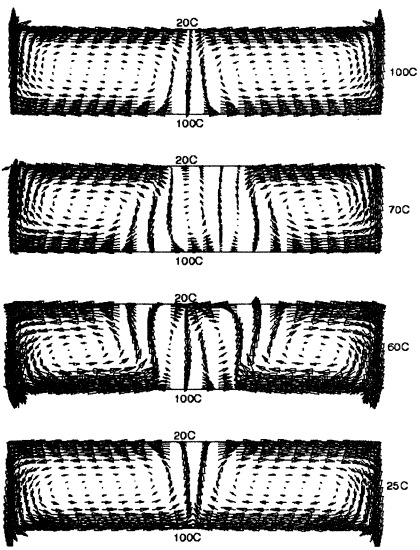

FIGURE 6 Steady-state velocity vectors in a 2D enclosure (aspect ratio 1:4) heated from below

The flow patterns induced in a compartment by a hot floor can be very complex [see for example Ref. 3]. Initially a hot, unstable layer (low-density gas under a high-density gas) forms above the hot floor, which then breaks up into convection cells or vortex rolls. The movement of this layer is controlled by buoyancy, thermal diffusion from the layer and viscous damping. The stability of this layer is characterised by the Raleigh number (Ra). When Ra exceeds a critical value (1708) the buoyancy of the layer dominates and the hot gases rise. This movement induces the formation of vortices as dense cool air falls to replace the warm rising air. Neighbouring pairs of vortices rotate in opposite directions. It should be noted that Ra exceeds the critical value when the depth of the hot layer reaches approximately 10mm.

For the bottom-heated configuration, for which there was no experimental information available, the results of the two-dimensional steady simulations for a 3m high rectangular

geometry are shown in figure 6. For these simulations, the bottom-side was set arbitrarily to a temperature of 100°C and for the topside an ambient temperature of 20°C was assumed. The temperatures of the vertical sides were varied between 20°C and 100°C.

It can be seen from the figure that the stability and structure of vortex rolls are sensitive to the side wall temperatures. An unstable four-vortex roll structure is found for temperatures of the vertical sides ranging between 60°C and 70°C. It can be noted that the predicted vortex rolls corresponding to side wall temperatures of 60°C rotate in opposite directions to those corresponding to side-wall temperatures of 70°C. The flow reversal in the rolling vortices occurs when the average mean temperature of the bulk fluid (T_b) becomes greater than the temperature of the side wall (T_w). An inner pair of secondary vortices appear when $T_b \approx T_w$. A more stable two-vortex roll structure is formed when $(T_b - T_w)$ is comparable to the temperature difference between the floor and the ceiling of the enclosure. Reducing the aspect ratio to 1:2 and then to 1:1 (similar to Compartment 2) leads to a more stable two-vortex roll structure (not shown). Increasing the aspect ratio to 1:8 resulted in a four-vortex roll structure (not shown), more pronounced than that observed for the aspect ratio of 1:4. The evolution and structure of the vortex rolls would influence time to detection, especially if detectors are located in the stagnation region of the flow. This was clearly evident from the transient development of the thermal convection currents (results not shown here) for the case of two-dimensional rectangular geometry (aspect-ratio 1:4) with boundary conditions as used in figure 7. The results showed an initial development of an unstable layer at floor level, its breaking up into multiple rising plumes and, as the flow approached the steady state, their convergence into the vortex roll structure shown in figure 7.

The above CFD predictions are based on standard (high Reynolds number) turbulence model (with buoyancy modification) and first-order upwind difference formulation. Figure 7 shows the results of the additional steady-state CFD simulations that were carried out using a second-order hybrid difference formulation both for standard turbulence model and the low Re k-ε turbulence model based on the work by Launder and Sharma [7]. The 2D geometry and boundary conditions used were the same as for the bottom case in figure 6 above. A total of 250 x 60 cells were used to represent the 12 m x 3 m geometry. The figure shows the comparison of the predicted Reynolds number distribution and velocity vector plots using standard and low Re k-ε turbulence models. It can be seen that the flow patterns are qualitatively similar for the two cases. Furthermore, the low Reynolds number, indicated by dark grey colour, covers only a small part, suggesting that the bulk of the flow is turbulent.

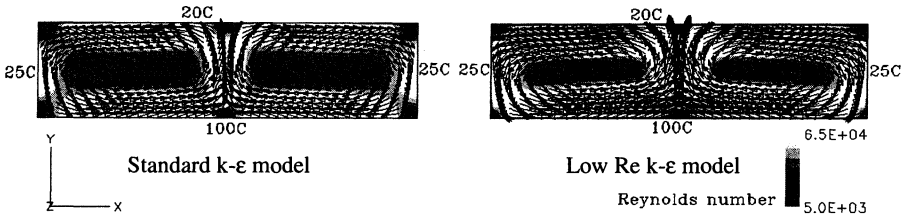

FIGURE 7 Comparison of predicted Reynolds number distribution and velocity vectors for the standard and low Re k-ε models respectively

A three-dimensional simulation of Compartment 2 without internal stiffeners and the storage rack, using the standard k-ε turbulence model and 100,000 cells, shows flow patterns similar to the corresponding two-dimensional case (see figure 8). Introduction of the internal stiffeners and the storage rack within Compartment 2 did not change the qualitative nature of the flow patterns.

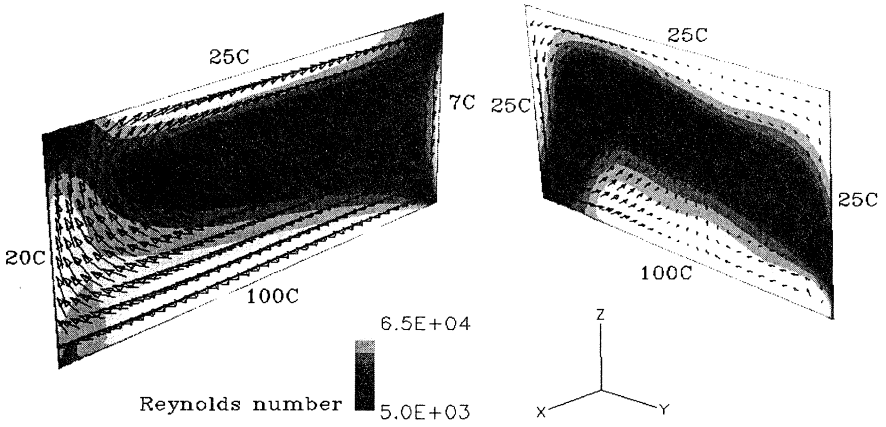

FIGURE 8 Steady-state velocity vectors in a 3D enclosure (aspect ratio c.1:1) subjected to heating from the side and from below

CONCLUSIONS

It has been shown that the CFD model has reproduced reasonably satisfactorily the thermal flow patterns in Compartment 2 both in the side-heated and bottom-heated configurations.

For Scenario B, the measured thermocouple temperatures are lower than those predicted by the CFD model because of the measurement errors incurred in the large sheathed thermocouples due to conduction losses to their supports in the experimental tests. It has been demonstrated that the model has reproduced the 'detection times' estimated from the thermocouple temperatures (after correcting for conduction losses) and the operation time of the detector in the experiment. In Scenario C, corresponding to the bottom-heated configuration, the transient heating of Compartment 2 from below leads to complex convection airflow patterns within the compartment. The structure and flow orientation of the rolling vortices is characterised by the temperature gradient between the bulk fluid temperature and the side wall temperature.

ACKNOWLEDGEMENTS

The work described in this paper forms part of a contract from the Ministry of Defence and is contributed by the permission of the Director Naval Architecture. It is published with the permission of the controller of Her Britannic Majesty's Stationery Office.

REFERENCES

1. Ostrach, S., "Natural Convection Heat Transfer in Cavities and Cells", in Proc. 7th Int. Heat Mass Transf. Conference, Munchen, Germany, vol. 1, 1987, p. 365.
2. Hanjalic, K., "Achievements and Limitations in Modelling and Computation of Buoyant Turbulent Flows and Heat Transfer", in Proc. 10th Int. Heat Transf. Conference, Brighton, UK, Vol. 1, Key Note paper SK-1, Published by I Chem. E, and Taylor & Francis, 1994.
3. Kenjeres, S. and Hanjalic, K., in Proc. 10th Symposium on Turbulent Shear Flows, The Pennsylvania State University, USA, 1995.
4. Connolly, R. J., Kirby, J. A. "Theoretical background to a computer program to predict the thermal response of materials to fire", Private communication, 1993.
5. Cox, G. and Kumar, S., Field modelling of fire in forced ventilation enclosures, Combus. Sci. Technol., 52, 7-23, 1987.
6. Lewis, M. J., Moss, J. B., Rubini, P. A. "CFD modelling of combustion and heat transfer in compartment fires", in Proc. of the 5th Int. Symp. on Fire Safety Science, Elsevier, pp. 463-474, 1997.
7. Launder, B. E. and Sharma, B. I., "Application of the energy-dissipation model of turbulence to the calculation of flow near a spinning disc", Letters in Heat and Mass Transfer, 1, 131-138, 1974.
8. Markatos, N. C. and Pericleous, K. A., "Laminar and turbulent natural convection in an enclosed cavity", Int. J Heat Mass Transfer, 27, 755-772, 1984.
9. Hottle, H. and Sarofim, A., Radiation heat transfer, McGraw-Hill, 1967.

APPENDIX A1: THERMOCOUPLE TEMPERATURE CORRECTION

The temperature correction for the sheathed thermocouple has been derived using the following assumptions:

- one-dimensional heat flow in the 1mm diameter sheathed thermocouple
- negligible radiation transfer
- linear temperature distribution along the wire
- uniform cross-section wire properties
- support has a large thermal mass and remains at a constant temperature
- negligibly small transient terms
- typical flow velocity of 0.25 m/s and a support temperature of 20°C

Considering the thermocouple as a long cylinder, with the sensing element recording the temperature occupying the last diameter of its length and the other end being at a fixed temperature, the heat transfer into the sensing element is:

$$Q_{in} = h\, A_s \Delta T \qquad \text{(A1.1)}$$

where h is a convective heat transfer coefficient, A_s the surface area and ΔT the temperature difference between the sensor and the surrounding gas $(T_g - T_s)$. The heat lost from the sensor head by conduction is:

$$Q_{loss} = A_w \, k \, \frac{dT}{dx} \tag{A1.2}$$

where A_w is the cross-sectional area of the cylinder, k the thermocouple conductivity and dT/dx the temperature gradient along the wire. The rate of heat accumulation at the sensor is:

$$Q_s = \rho \, c_p \, V_s \, \frac{dT_s}{dt} \tag{A1.3}$$

where ρ is the wire density, c_p is specific heat capacity, V_s the volume of the sensor region and dT_s/dt the rate of change of the sensor temperature. Constructing a heat balance gives:

$$Q_{in} = Q_{loss} + Q_s \tag{A1.4}$$

Putting the areas and volumes in terms of the thermocouple diameter, d, and transposing gives:

$$T_g = \frac{l}{h}\left[\rho c_p d \frac{dT_s}{dt} + \frac{k}{4l}(T_s - T_E)\right] + T_s \tag{A1.5}$$

where l is the distance between the sensing tip of the thermocouple and the support which is maintained at a fixed temperature T_E. Assuming that temperature changes with time are relatively slow, dT_s/dt becomes small and the expression reduces to:

$$T_g = T_s\left[1 + \frac{k}{4hl}\right] - \frac{k}{4hl} T_E \tag{A1.6}$$

The heat transfer coefficient for a cylinder can be estimated from $h = kNu/d$, where Nu is the Nusselt number calculated from [9]:

$$Nu = 0.42 \, Pr^{0.2} + 0.57 \, Pr^{0.33} \, Re^{0.5} \tag{A1.7}$$

where Pr, the Prandtl number is $\mu c_p/k$ and Re, the Reynolds number, is $\rho v d/\mu$.

The typical flow velocity (v) near the deckhead thermocouples is of the order of 0.3m/s and the length of the thermocouple was approximately 150mm. Assuming the point of contact between the thermocouple and the support was at a temperature of 20°C then the gas temperature can be calculated from:

$$T_g = 2.3 \, T_s - 26 \tag{A1.8}$$

This expression can be used either to estimate the gas temperatures in the experiment from the thermocouple data or to estimate the temperature of thermocouples exposed to gas temperatures calculated by JASMINE. When a thermocouple indicates a temperature of 68°C this corresponds to a gas temperature of 130°C and a gas temperature of 68°C gives a thermocouple temperature of 41°C.